

Reports

Mariners 6 and 7: Radio Occultation Measurements of the Atmosphere of Mars

Abstract. Radio occultation measurements with Mariners 6 and 7 provided refractivity data in the atmosphere of Mars at four points above its surface. For an atmosphere consisting predominantly of carbon dioxide, surface pressures between 6 and 7 millibars are obtained at three of the points of measurement, and 3.8 at the fourth, indicating an elevation of 5 to 6 kilometers. The temperature profile measured by Mariner 6 near the equator in the daytime indicates temperatures in the stratosphere about 100°K warmer than those predicted by theory. The measurements of Mariner 6 taken at 79°N at the beginning of polar night indicate that conditions are favorable for the condensation of carbon dioxide at almost all altitudes. Mariner 7 measurements taken at 58°S in daytime and 38°N at night also show that carbon dioxide condensation is possible at altitudes above about 25 kilometers. Measurements of the electron density in the ionosphere show that the upper atmosphere is substantially warmer than it was in 1965, possibly because of increased solar activity and closer proximity to the sun.

The successful flights of Mariners 6 and 7 provided opportunities for four more occultation measurements of the atmosphere, ionosphere, and surface configuration of Mars, thus increasing the amount of data obtained at Mars with the radio occultation method by more than 200 percent. Mariner 6 made its closest approach to Mars at 05:19:06 U.T. on 31 July. Approximately 20 minutes later it disappeared from the view of the earth and its radio beam was interrupted by the surface of Mars at a point near Maridiani Sinus (latitude 4°N, longitude 355°E). The local time at this point was 15:40, and the solar zenith angle was approximately 57 degrees. At the moment of occultation the spacecraft was about 9800 km from the limb. After remaining in occultation for about 20 minutes, the spacecraft emerged in the vicinity of the north polar region of Mars, at a latitude of 79°N and a longitude of 84°E. The local time at that point was 21:40, and the solar zenith angle was about 107 degrees. At this time the spacecraft was approximately 17,400 km from the limb.

Mariner 7 arrived in the vicinity of Mars approximately 5 days later, making its closest approach at 05:00:49 U.T. on 5 August. Some 19 minutes later its S-band radio beam was cut by the surface of Mars in the area of Hesperontus at a latitude of 58°S and

a longitude of about 30°E. The local time there was approximately 14:20, and the solar zenith angle was approximately 56 degrees. At that time the Mariner 7 spacecraft was about 9050 km from the limb. About 30 minutes later the spacecraft's radio signal emerged from behind Mars in the vicinity of Amazonis and Arcadia at a latitude of 38°N and a longitude of 211°E. The local time there was 03:00 and the solar zenith angle about 130 degrees. At that time the spacecraft was about 20,180 km from the limb.

During each entry and exit of the radio beam through the atmosphere of Mars, the frequency and amplitude of the signal received afterward at the earth were changed by the effects of refraction upon the propagation of the radio signal. These effects are treated in more detail in descriptions of previous radio occultation experiments (1, 2). The methods of obtaining and analyzing the data have been described (3), and the following is only an abbreviated description of the procedures used during the present experiment. For both Mariner 6 and Mariner 7, the entry into occultation was performed in a two-way mode of operation, in which a frequency referenced to a rubidium standard at the Deep Space Net (DSN) station is transmitted to the spacecraft, where it is coherently retransmitted. The exit data, however, were obtained

in the one-way mode of operation, in which the spacecraft's transmitter is referenced to its on-board crystal oscillator. The received signal was passed through the standard phase-locked-loop receiver, and the record of non-destructively counted Doppler was recorded by the Tracking Data Handling System. This constituted the closed-loop data, on which the results described in the present paper are based. Simultaneously, the signal was passed through a special open-loop receiver, having an audio passband of approximately 5 khz. It produced a frequency-translated version of the received signal which was recorded on an analog tape recorder, as well as being digitized in real time and recorded on digital magnetic tape. These data are referred to as the open-loop data, which have not yet been thoroughly analyzed.

For the Mariners 6 and 7 occultation experiments, Deep Space Station (DSS) 14 (Mars) and 12 (Echo) at the Goldstone, California, complex were instrumented with open-loop receivers, and the open-loop data from DSS 14 were transmitted over a microwave link to DSS 13 (Venus) where they were digitized in real time and recorded. Closed-loop Doppler data were also taken at DSS 14 and DSS 12, as well as DSS 41 in Woomera, Australia. The open-loop receiver is necessary to insure instantaneous reception of the data as the spacecraft reemerges from behind the planet. This is difficult to accomplish with the phase-locked-loop receiver because of its finite lockup time. Another purpose of the open-loop receiver is the obtaining of amplitude data that cannot be obtained from the locked-loop receiver because of the long time constant of its AGC circuit. The bandwidth of the open-loop receiver was selected on the basis of the projected Doppler frequency rates due to the motion of the spacecraft. These rates, together with the fact that it was undesirable to retune the receiver within 3 minutes of occultation, led to an open-loop passband selection of approximately 5 khz. In order to insure precise tuning of the open-loop receivers, as well as to preserve their frequency-translation integrity, all the local oscillator frequencies were synthesized from a rubidium standard. An audio phase-locked-loop receiver as well as a spectrum analyzer and other test equipment were provided in the open-loop system to give a real time indication of the signal being received and recorded. This test equipment could be switched between the

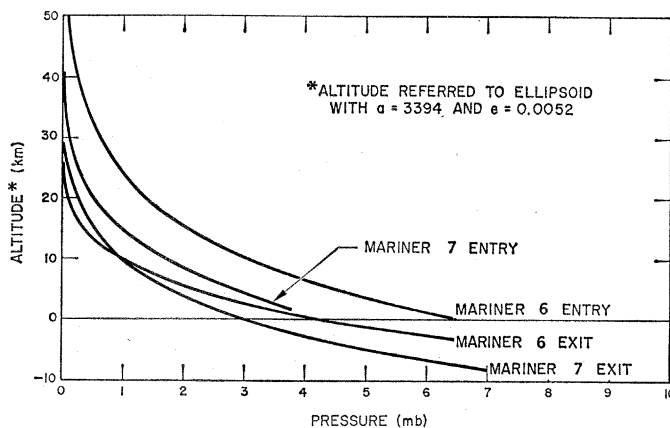
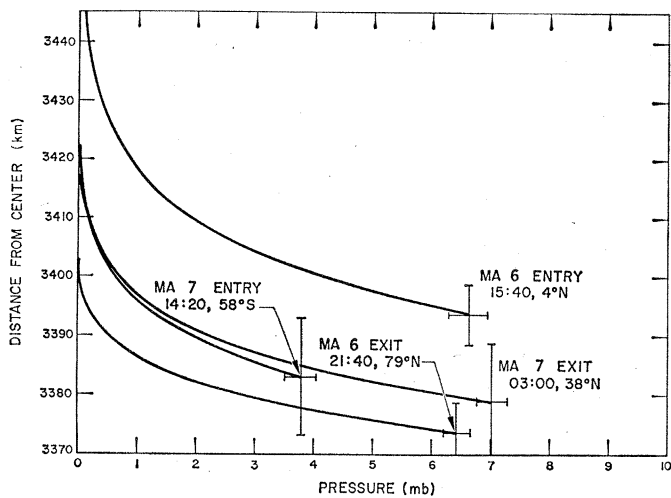


Fig. 1 (left). Pressure as a function of distance of the radio beam from the center of Mars from the Mariner 6 and 7 measurements. Fig. 2 (right). Pressure as a function of altitude with respect to a reference ellipsoid with $a = 3394$ km and $e = 0.0052$.

output of the open-loop receiver and the various reproducing units of the analog tape recorders. A 20 kHz test-tone referenced to a rubidium standard was added to the data channel prior to recording to insure that the frequency recorded by the analog recorders was not distorted by more than a fraction of a hertz. Later this test tone was used as a time base for keying the digitizers sampling the data. The analog recordings were used primarily as backups to the real-time digital recordings which, because of system constraints, had to be obtained over a microwave link.

The digital open-loop data are passed through the Decimation and Spectral Analysis programs and the Digital Phase-Lock Receiver program which produces a record of the frequency and amplitude of the received signal sampled at arbitrary intervals of time. The frequency is then compared with pre-

dictions based on the orbit of the spacecraft, and the differences in frequency constitute the open-loop residuals. The closed-loop data, consisting of the biased Doppler counts, are processed by the Orbit Determination program, which compares the counts to predictions based on an orbit, and the differences constitute the closed-loop residuals. Because of system limitations, the maximum sampling frequency is one sample per second. The residuals are then passed through a Data Preparation program, which removes any bias or drift that might be present and integrates to obtain a record of the total phase path change due to refraction effects in the ionosphere and atmosphere. From there, the data go to the Inversion program which makes use of trajectory data provided by the Double Precision Trajectory program and performs integral inversion (4) of the data

to obtain the refractivity profile. This profile is then used to compute the electron density in the ionosphere and the pressure, temperature, and other parameters of the lower atmosphere.

The profile of refractivity, as obtained by inversion, can be directly interpreted in terms of the electron density in the upper atmosphere; however, in order to obtain profiles of density, pressure, and temperature in the lower atmosphere, an assumption of the composition must be made. In deriving the results presented here, we assumed that CO_2 is the predominant constituent in the Martian atmosphere. This assumption is based on the results of ground-based spectroscopy, as well as on the results of other experiments aboard Mariners 6 and 7 (5). The temperature and pressure profiles shown in Figs. 1 through 4 were obtained for a composition of 90 percent CO_2 and

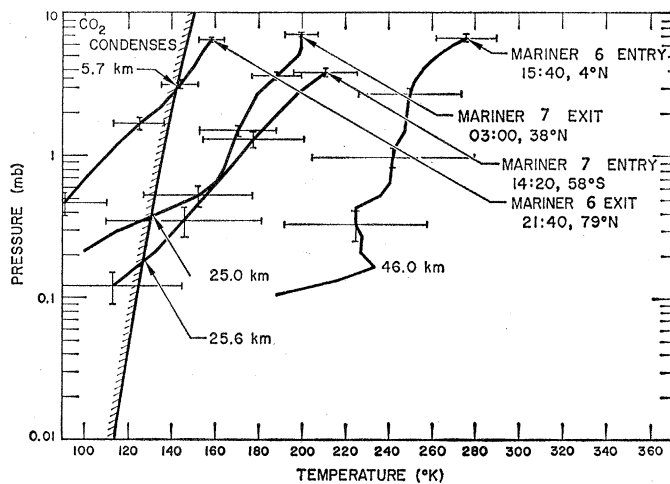
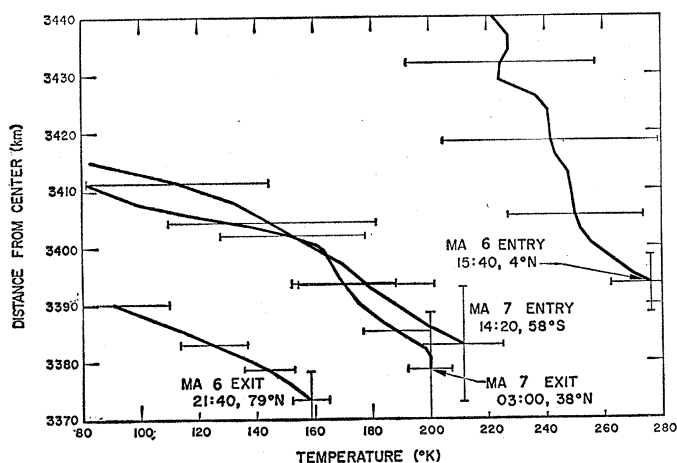


Fig. 3 (left). Temperature as a function of distance from the center of Mars. The uncertainty boundaries include only the effect of estimated uncertainty in the determination of refractivity. Fig. 4 (right). Pressure as a function of temperature for all profiles derived from Mariner 6 and Mariner 7 measurements. The region to the left of the shaded boundary is favorable for the condensation of CO_2 . The numbers referred to in the boundary denote altitude at which the boundary is reached.

10 percent argon. They are valid as long as the composition remains predominately CO_2 . Should it, however, be necessary to revise the estimate of CO_2 downward and to fill the remaining portion with some less refractive gas, the results would have to be substantially changed. For instance, if the composition should change to 80 percent CO_2 and 20 percent neon, the temperatures at all altitudes would decrease by approximately 10 percent. A more reliable composition will emerge when the data from the Mariners 6 and 7 spectrometer experiments are completely analyzed.

Figure 1 shows the profiles of pressure as a function of the distance of the radio beam from the center of Mars for all four of the occultation measurements. The error limits on the pressure measurements are based on an assumption of a 0.05 N-unit uncertainty in the refractivity. It should be pointed out that these error limits do not include the possible effects of an incorrectly assumed composition. The uncertainties in the vertical scales depend on the accuracy of the knowledge of the orbital paths of Mariners 6 and 7. At the time these results were computed, the uncertainties in the orbits produced an uncertainty in the knowledge of the position of the radio beam with respect to the center of Mars of ± 10 km for Mariner 7, and about ± 5 km for Mariner 6. It is expected that these uncertainties will be reduced to about ± 1 km when the orbit becomes more precisely known. For an atmosphere in hydrostatic equilibrium, the pressure should be approximately equal on a gravitational equipotential surface. Figure 2 shows the derived pressure profiles plotted as a function of altitude above a mean reference ellipsoid having an equatorial radius of 3394 km and an ellipticity of 0.0052. This corresponds to a figure of Mars inferred from dynamical measurements of oblateness. If the reference ellipsoid were correct, and if the radial distance scales of the original pressure profiles were correct, then one would expect the profiles to lie very close to one another. The evident disagreement between the profiles in Fig. 2 indicates that this is not yet the case. However, when the radial distance coordinates are established to a greater degree of precision, it will be possible to use these measurements to compute the reference equipotential gravitational surface of Mars.

It is evident from Figs. 1 and 2 that three of the four measurements of pres-

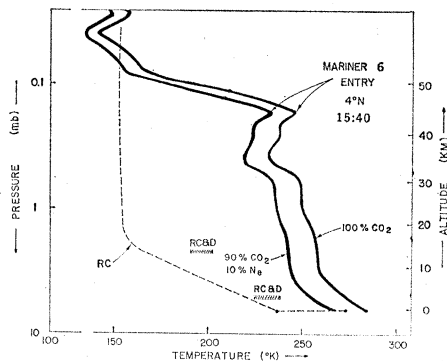


Fig. 5. Temperature as a function of pressure in the atmosphere of Mars at the entry point of Mariner 6 (thick line) for two assumed compositions. The broken line represents temperature distribution calculated for radiative convective equilibrium (RC) by Gierasch and Goody (7), also for the entry point of Mariner 6. The horizontal bars marked RC&D are the temperature values estimated for two pressure levels when atmospheric dynamics is also taken into account; adapted from Leovy and Mintz (9).

sure at the surface fall between 6.4 and 7 mb. Thus it seems that these measurements taken over widely different latitudes and longitudes on Mars appear to lie close to a common equipotential surface. The fourth measurement, however, taken in the area of Hellespontus (58°S) yields a pressure of only 3.8 mb, an indication that the surface feature which interrupted the radio signal at that point lies at some 5 to 6 km above the mean ellipsoid in the vicinity of which the other three occultation observations were taken. For Mariner 6, the radius measured at 4°N differs from that measured at 79°N by approximately 20 km. Since the pressures measured at these two points are very nearly equal, one can assume that one is measuring the shape of the gravitational equipotential surface, and

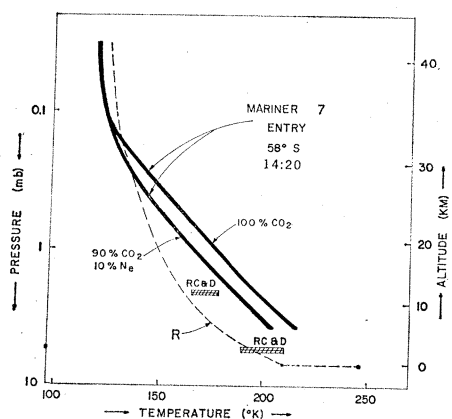


Fig. 6. Same as Fig. 1 but for Mariner 7 entry. The radiative curve (R) is adapted from Ohring and Mariano (12).

thus one may conclude that the physical surface of Mars has a shape similar to the shape of the gravitational equipotential surface predicted by the dynamical oblateness of Mars as opposed to the optically observed flattening.

The profiles of temperature as a function of distance from the center of Mars for all four measurements are shown in Fig. 3. The uncertainty boundaries again have been established if we assume an uncertainty of .05 N units in the refractivity, and they do not reflect possible errors due to uncertainties in composition. The pressure and temperature profiles are cross-plotted in Fig. 4.

The vertical distributions of temperature in the atmosphere of Mars, as shown in Figs. 3 and 4, have been deduced on the assumptions that the atmosphere is in hydrostatic equilibrium and that the ideal gas law is valid. The thermodynamics of atmospheric condensation has not been taken into account. For this reason, in three of the four cases shown in Fig. 4, especially that of Mariner 6 exit, the atmospheric temperatures are substantially lower than the condensation temperatures of CO_2 , implying that the atmosphere at these levels is supersaturated. In reality, if suitable condensation nuclei are present, condensation should occur, releasing latent heat, and thereby raising the atmospheric temperatures. If it is assumed that radiational cooling is balanced by transport of energy by circulation, then the atmospheric temperatures should closely follow the saturation temperature curve shown in Fig. 4. As this may well be the case, particularly in the polar night on Mars, it seems more appropriate that, when the derived temperatures fall below the condensation temperature of CO_2 , the "saturation" law, rather than the ideal gas relation, be used to deduce the temperature and pressure profiles. When the refractivity data are reduced in this manner, the atmospheric temperatures are never lower than the saturation temperatures of CO_2 and have the effect of raising the surface pressure by a few percent. The results of this analysis are shown in Figs. 5, 6, 7, and 8.

Each of these figures shows two profiles, one for 100 percent CO_2 , and the other for 90 percent CO_2 and 10 percent Ne. Though it is generally accepted that CO_2 is the major constituent of the martian atmosphere, its exact concentration has not yet been established. Estimates range from 60 to 100 percent. This poses an interesting question regarding the identity of the

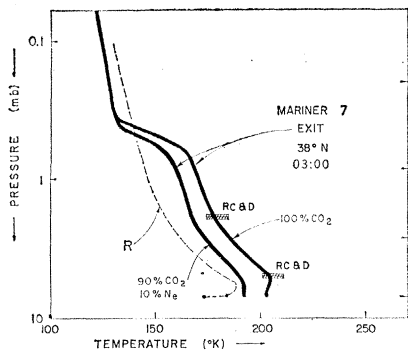


Fig. 7. Same as Fig. 1 but for Mariner 6 exit. The radiative curve is after Gierasch and Goody (7).

other constituents in the atmosphere of Mars. The problem has bearings on the origin of the martian atmosphere. It has been argued that if the present atmosphere of Mars is a remnant of a primordial atmosphere, which once had the solar composition, then after the escape of H_2 and He the atmosphere should contain 60 percent CO_2 , 25 percent Ne, and about 15 percent N_2 (6).

However, if the present atmosphere of Mars is the result of outgassing from the interior, as with the earth, then by analogy with the earth Ne should be completely absent and the atmosphere should contain about 95 percent CO_2 , 2 to 3 percent N_2 , and traces of Ar, depending upon the extent of outgassing. The presence or absence of Ne in the atmosphere of Mars is therefore an important datum for the understanding of the problem of the origin of the martian atmosphere. Interestingly, in the interpretation of the refractivity data in terms of atmospheric number density, it is also the presence of Ne which makes a substantial difference in the resulting temperature

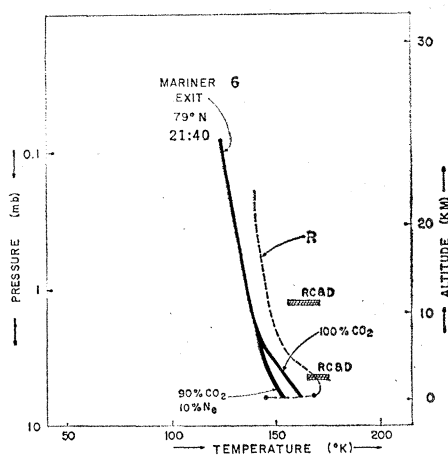


Fig. 8. Same as Fig. 1 but for Mariner 7 exit. The radiative curve (R) is adapted from Ohring and Mariano (12).

profiles. The addition of only 10 percent Ne in the atmosphere makes the derived temperatures substantially lower than those for 100 percent CO_2 because the refractivity of Ne is about six times smaller than that of CO_2 .

The variety and range of the temperature profiles shown in Figs. 5, 6, 7, and 8 reveal several important and unexpected aspects of martian meteorology. In the following discussion, the salient features of these results are emphasized by comparing each of the observed temperature profiles with the atmospheric temperatures predicted by existing theoretical models of the martian atmosphere.

The thermal structure of the atmosphere of Mars has been the object of several comprehensive studies during the last few years. Notably, it has been argued that because CO_2 is the major constituent of the atmosphere and the total surface pressure is only about 10 mb, radiative heat exchange should dominate over convective and advective energy transport (7, 8). Consequently, the martian atmosphere should be coupled radiatively to the surface much more strongly than is the terrestrial atmosphere, and the temperature distribution in the atmosphere above a given point on the martian surface should be determined essentially by local radiative-convective balance. Furthermore, because the atmosphere is optically thin, one might expect a sharp temperature discontinuity between the atmosphere near the surface and the surface itself of as much as $+70^\circ K$ at midday and $-50^\circ K$ at night (7, 8).

In reality, however, atmospheric circulation on a planetary scale would modify such a thermal structure to some extent. Detailed numerical computations by Leovy and Mintz (9) indicate that the net effect of advection is to decrease the magnitude of the temperature discontinuity at the ground and to raise the atmospheric temperatures so that the lapse rate becomes subadiabatic at the equator and close to zero at the poles.

In Figs. 5, 6, 7, and 8 the measured temperature distributions are compared with temperature profiles calculated for similar conditions, taking into account radiative transfer alone (R), and both radiative and convective exchange (RC). Also indicated are the temperatures anticipated at two different levels in the atmosphere if all three processes—radiation, convection, and dynamics (RC&D)—are considered.

Figures 5 and 6 correspond to day-

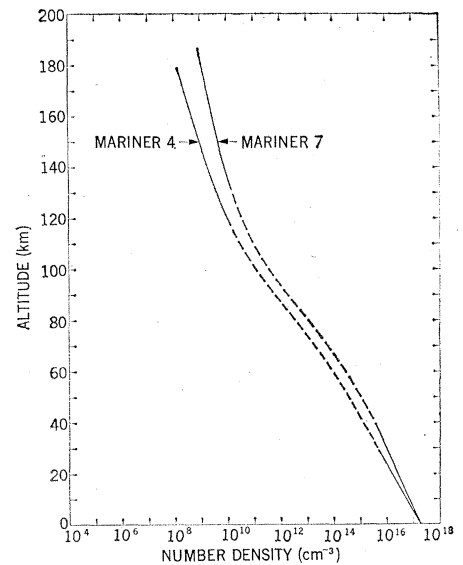


Fig. 9. Number density versus altitude. The Mariner 4 (1965) data were obtained near $50^\circ S$, at 13:00 local time in late winter. The solar zenith angle was 67 degrees. The Mariner 7 (1969) data were obtained near $58^\circ S$ at 14:30 local time in early spring. The solar zenith angle was approximately 56 degrees.

time, while Figs. 7 and 8 correspond to nighttime on Mars. Comparison of the observed temperature structures with the theoretical models for the four different locations indicates the following important features.

1) The atmospheric temperatures observed at the equator in midafternoon are significantly higher than the predicted temperatures up to an altitude of 40 km. The observed gradient in the lower atmosphere is subadiabatic and this suggests the presence of a tropopause at an altitude of 9 km. The temperature found in the equatorial strato-

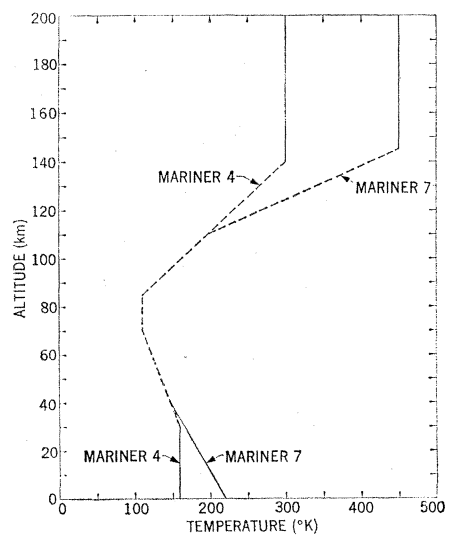


Fig. 10. Temperature versus altitude.

sphere is 100°K higher than that predicted from radiative transfer alone. The observations also indicate a sudden decrease of temperature at 0.2 mb, with the temperature gradient becoming superadiabatic. However, this is the least certain feature of the temperature profile.

2) The temperature distributions in midafternoon near the southern polar cap (Fig. 6) and in the subtropics in the early morning hours (Fig. 7) appear to be quite close to the profiles predicted when atmospheric dynamics were taken into account.

3) At 79°N, where the polar night is just beginning, the observed temperature profile, if interpreted with the assumption of saturation and condensation of CO₂ in the atmosphere, suggests that condensation of CO₂ is occurring at practically all heights in the atmosphere.

The case of the tropical atmosphere in daytime (Fig. 5) is the most interesting. At the equator, the atmosphere is much warmer than expected. For the 100 percent CO₂ case, the atmospheric temperature near the surface is about 283°K. However, the actual surface temperature measured by the infrared radiometer near the point of occultation is about 275°K (10), indicating an inconsistent negative temperature discontinuity of 8°K. For the case with 10 percent Ne, the atmospheric temperature near the ground is 268°K and the temperature discontinuity is only 7°K, differing markedly from the predicted value of Gierasch and Goody. In addition, the problem still remaining is that the atmosphere is substantially warmer than that suggested from the theoretical calculations. Either the opacity of the atmosphere is much higher than that estimated from the various CO₂ band models, or a significant amount of solar radiation is deposited in the middle atmosphere by absorption in the near-infrared bands of CO₂, or a combination of both.

The Mariner 1969 refractivity measurements in the upper atmosphere of Mars yielded results similar to those obtained with the Mariner 4 in 1965 (1). On the dayside, the main layer was now located near 135 km altitude, and it had a peak density of approximately 1.7×10^5 electron/cm³. The minor layer was observed near an altitude of 110 km. The topside plasma temperature was 400° to 500°K on the assumption that CO₂⁺ is the principal ion. No ionization was detected on the dark side of the planet (11).

Figures 9 and 10 show the density and temperature profiles deduced from the high latitude dayside measurements made with Mariners 4 and 7. The atmospheric models illustrated in these figures are based on the assumption that the main ionization layer is an F₁ region produced by solar extreme ultraviolet. Solid curves represent results derived from the refractivity data. Stippled curves indicate interpolation between the measurements made in the ionosphere and the neutral atmosphere. The figures show both the upper and the lower atmosphere to be warmer now than in 1965. The temperature increases are presumably due to seasonal changes, increased solar activity, and a 10 percent reduction in the distance to the sun.

ARVYDAS KLIORÉ
GUNNAR FJELDBO
BORIS L. SEIDEL

Jet Propulsion Laboratory,
California Institute of Technology,
Pasadena

S. I. RASOOL
Institute for Space Studies,
Goddard Space Flight Center,
New York

References and Notes

1. A. Kliore, D. L. Cain, G. S. Levy, V. R. Eshleman, G. Fjeldbo, F. D. Drake, *Science* **149**, 1243 (1965).
2. A. Kliore, D. L. Cain, G. S. Levy, in *Space Research VI—Moon and Planets*, A. Dollfus, Ed. (North-Holland, Amsterdam, 1967), p. 226; G. Fjeldbo and V. R. Eshleman, *Planet. Space Sci.* **16**, 1035 (1968).
3. G. S. Levy, T. Otoshi, B. L. Seidel, *Inst. Elect. Electron. Eng. I.E.E.E. Trans. Instr. Meas.* **16**, 100 (1967).
4. G. Fjeldbo and V. R. Eshleman, *J. Geophys. Res.* **70** (1965).
5. C. A. Barth, W. G. Fastie, C. W. Hord, J. B. Pearce, K. K. Kelly, A. I. Stewart, G. E. Thomas, G. P. Anderson, O. F. Raper, *Science* **165**, 1004 (1969).
6. S. I. Rasool, S. Gross, W. E. McGovern, *Space Sci. Rev.* **5**, 565 (1966); S. H. Gross, W. E. McGovern, S. I. Rasool, *Science* **151**, 1216 (1966).
7. P. J. Gierasch and R. M. Goody, *Planet. Space Sci.* **16**, 615 (1968).
8. R. Goody, *Comments Astrophys. Space Phys.* **1**, 128 (1969).
9. C. Leovy and Y. Mintz, *Rand Corporation Memorandum RM-5110-NASA*, December 1966; *J. Atmos. Sci.*, in press.
10. G. Neugebauer, G. Munch, S. C. Chase, Jr., H. Hatzenbeler, E. Miner D. Schofield, *Science* **166**, 98 (1969).
11. G. Fjeldbo, A. Kliore, B. Seidel, *Radio Sci.*, in press.
12. G. Ohring and J. Mariano, *J. Atmos. Sci.* **25**, 673 (1968).
13. We thank the Mariner Project and DSN personnel at Jet Propulsion Laboratory who, through their competence, guaranteed the flawless acquisition of our data. In particular we thank D. Nixon for help in the acquisition and M. P. Milane, Joan Jordan, and Nancy Hamata for help in the reduction of the data. Special thanks are due to P. J. Gierasch and C. Leovy as well as R. Stewart for discussions helpful to the interpretation of our results. This work presents the results of one phase of research carried out at JPL, California Institute of Technology, under NASA contract NAS 7-100.

31 October 1969

Man-Made Carbon-14 in Deep Pacific Waters: Transport by Biological Skeletal Material

Abstract. *Calcareous particles present in Pacific waters at depths of 50 to 3500 meters were collected by filtering seawater through spongin matrix. The specific activity of carbon-14 could be measured in two of these collections from depths of 2300 and 3500 meters. The ratios of carbon-14 to carbon-12 correspond to values observed in surface waters in recent years as a result of the addition of man-made carbon-14, thus indicating that the calcareous particles resulted from recent biological productivity. The results are related to the mean settling rates and the sizes and dissolution rates of biogenic calcareous particles in transit through a seawater column.*

During the Nova Expedition of the Scripps Institution of Oceanography, experiments were carried out between Hawaii and New Zealand in which spongin matrix treated with ferric hydroxide was used for the extraction *in situ* of trace elements from seawater (1) with stainless steel samplers (2). Seawater was flushed through the matrix at the desired depth by raising and lowering the sampler for 10 to 15 hours at mean speeds of about 10 m/min. The samplers descended to the profile depth in an orientation which did not allow water to flow through the matrix. Corrosion of a magnesium strip at the profile depth swung the samplers into the correct orientation for the free flow of water.

In the expectation that the matrix could also serve as a collector of particulate calcareous matter, we treated portions of the seawater-treated matrix with hydrochloric acid in a vacuum system and measured the amount of carbon dioxide evolved. All samples yielded measurable amounts of CO₂ and two of the deep samples yielded sufficient carbon dioxide to permit measurements of C¹⁴ activity. The results of these measurements, carried out by the use of procedures discussed by Agrawal *et al.* (3), are given in Table 1.

As a check on any contamination of CO₂ introduced by the direct pickup of impurities in the atmosphere by the ferric hydroxide-loaded spongin, we analyzed control samples of spongin matrix; no measurable carbon dioxide was found. Laboratory experiments with aqueous solutions of carbonate, bicarbonate, and CO₂ (gas) showed that